Hindawi Publishing Corporation
Advances in Materials Science and Engineering
Volume 2011, Article ID 987671, 7 pages
doi:10.1155/2011/987671

Research Article

Thermal Effect on Structure of Silver in Ion-Exchanged Soda-Lime Glasses and Aluminum-Doped Zinc Oxide Films

Paul W. Wang,[1] Yanfeng Jiang,[2] Jin-Cherng Hsu,[3] Yu-Yun Chen,[4] Yung-Hsing Lin,[4] and Huang-Lu Chen[4]

[1] *Department of Physics, Bradley University, 1501 W. Bradley Avenue, IL 61625, USA*
[2] *Department of Microelectronics, North China University of Technology, 5 Jinyuanzhuang Road, Shijingshan District, Beijing 100144, China*
[3] *Department of Physics, Fu-Jen Catholic University, 510 Chung-Cheng Road, Hsin-Chuang 242, Taiwan*
[4] *Graduate Institute of Applied Science and Engineering, Fu Jen Catholic University, 510 Chung-Cheng Road, Hsin-Chuang 242, Taiwan*

Correspondence should be addressed to Paul W. Wang, pwang@bradley.edu

Received 6 April 2011; Revised 20 June 2011; Accepted 26 June 2011

Academic Editor: Joseph Lai

Heat treatment is commonly used during device processing in order to achieve specific functionalities of the devices. How a series of heat treatment applies to accomplish this goal can be found in the literature. However, specific properties of the devices after the treatment are more emphasized than the details of the structural modifications in the industrial applications. In this paper, it is intended to illustrate the fundamental changes in the structure due to heat treatment which result in the desired physical properties of the devices. Two study cases, Ag ion-exchanged soda-lime glasses and aluminum doped ZnO (AZO) films, were illustrated. The changes in chemical states, the structural modification during and after heat treatment are explored. By understanding how the metallic Ag formed and accumulated during annealing, an optimum heat treatment to grow the proper size and density of silver quantum dots in the films are possible. Post annealing effect on the AZO films shows that the crystallinity, the peak positions shifts, and grain sizes were changed after annealing. Both illustrated cases indicate thermally induced changes in chemical state, the stress release, and rearrangement of atoms in materials during and after annealing.

1. Introduction

Heat treatment is commonly used to change the properties of metals, such as to soften or harden, to relieve the internal stress and to modify the grain structures [1]. Heat treatment is also widely applied to semiconductor and optoelectronic devices. For example, in order to activate the electrical properties of ultralow energy ion implanted donors and acceptors in silicon, recrystallize the damaged silicon crystal caused by ion implantation [2], and to maintain the shallow dopant depth profile similar to as-implanted profile, a subsequent rapid thermal annealing, at high ramp rate (400°C/s), short time (<1 s), and high temperature (>1000°C) annealing is required [3]. The other example is that heat treatment is used to form the quantum dots/nanocrystals after metal ions implanted in MgO, SiO_2 and Si [4–6]. Moreover, the size and density of the quantum dots in the film were closely correlated to the annealing temperatures [7]. Even though there are so many reports of heat treatment on different materials, the specific properties of the devices after the treatments are more emphasized than the consequence of the structural modifications in the industrial applications.

Chemical states of metal atoms in optical materials play an important role in optical properties since they control the polarizability of electrons in the metal-ligand matrix under light exposure and therefore, the refractive indices of materials are greatly affected by them. They also indicate how the metal atoms form different bonds to its neighboring atoms [8]. As a result, in this paper, the structural modifications, that is, chemical states of Ag in Ag ion-exchanged soda-lime glasses and the structure of AZO films were investigated by X-ray Photoelectron Spectroscopy (XPS) and X-ray Diffractometer (XRD) during and after the heat treatment.

2. Experiment

2.1. Silver in Ion-Exchanged Soda-Lime Glasses. Silver ion-exchanged soda-lime glasses were prepared by using commercially available soda-lime glasses (72.6% SiO_2, 15.4% Na_2O, 6.3% CaO, 3.87% MgO, 1.63% Al_2O_3, and 0.2% Fe_2O_3) submerged into a molten $AgNO_3$ salt at 450°C for 45 min. Samples were examined by the Perkin-Elmer PHI model 560 system for XPS analyses. The X-ray was Mg Kα line (1253.6 eV), produced by 15 KV electron impact on a magnesium anode at a power level of 300 W and was used as an excitation source. The pass energy was set at 25 eV to provide a 0.5 eV resolution. The heat treatment of the ion-exchanged glass sample was carried out by using a button heater underneath the metal plate on which the sample was mounted. The sample was heated in 50°C increments up to 450°C, and the photoelectrons were collected by a double-pass cylindrical mirror energy analyzer at various sample temperatures. The time that the sample was held at each temperature was 30 min which allowed the collection of XPS data. In order to separate the metallic state from an Ag3d XPS peak, a pure metal silver foil with native oxide was studied before and after 2.8-keV argon ion sputtering for 1 h by XPS. Once the spectra of the metallic silver and oxidized silver from sputtering study had been obtained, the curve fitting technique was applied to resolve the metallic and the oxidized state of Ag in Ag3d spectra. The peak position in the XPS spectrum is the binding energy of the emitted photoelectron which represents a certain chemical state. The relative surface concentration of the chemical state of that element was calculated from the integrated area of XPS peak with the atomic sensitivity factor taken into account. The calibration of the binding energy due to surface charging even after the surface was neutralized by a low energy electron flood gun was done, similar to other researchers [9], by assuming the binding energy of adventitious carbon 1s photoelectrons located at 284.6 eV.

2.2. Aluminum-Doped Zinc Oxide Films. The apparatus of the ion beam sputtering deposition (IBSD) system included an ion source used to produce an energetic ion beam for sputtering metal materials off from target and then to deposit the metal oxide onto a substrate in oxygen ambiance. The ion source of this system was made by Veeco Inc. equipped with 3 cm diameter molybdenum grids. The details of the IBSD setup was previously published [10]. The high purity 99.99% zinc and aluminum metal targets with the same sizes of 12 cm×10 cm×1 cm were mounted side by side on a water-cooled copper block as shown in our previous publication [11]. The incident angle between ion beam and the normal of target surface was 45°.

Prior to mounting the substrates and pumping down the system, the 1.3 cm×1.3 cm B270 glass substrates were cleaned by alcohol in an ultrasonic cleaner and blown dry by nitrogen gas. The chamber was cryogenically pumped down to a base pressure of 6×10^{-6} Torr. Then the targets were cleaned *in situ* by the ion beam with a shutter to cover the substrate for 30 mins. The ion-beam voltage was kept at 1000 V with the ion-beam current at 20 mA during deposition. Argon was fed into the ion source as a working gas and oxygen was fed into the chamber at a partial pressure of 1.2×10^{-4} Torr which was examined by our previous study of deposition ZnO film [12]. The total pressure of the chamber was maintained at 2.4×10^{-4} Torr. The AZO thin films were deposited onto B270 glass substrates at room temperature.

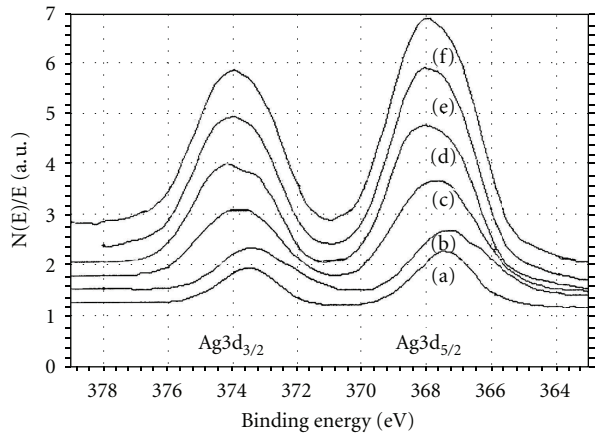

FIGURE 1: The *in situ* XPS spectra of $Ag3d_{3/2}$ and $Ag3d_{5/2}$ from ion-exchanged glass at various sample temperatures: (a) 20°C, (b) 100°C, (c) 200°C, (d) 300°C, (e) 400°C, and (f) 450°C.

By adjusting the positions of two targets with respect to the Ar ion beam, the relative concentrations of Al and Zn in the films were controlled by the sputtered area ratio of the Al to Zn target. The as-deposited AZO films were annealed in air at 100, 200, 300, and 400°C, respectively. An X-ray diffraction (XRD) apparatus (Rigaku Multiflex) with a Cu Kα line (1.54055 Å) was used to examine the structure of the films after annealing. The d-spacing between adjacent crystalline planes, grain sizes in the film, and the stress in the films was deduced from the diffraction angles and the full width at half maximum (FWHM) of the diffraction peak.

3. Results and Discussion

3.1. Silver in Ion-Exchanged Soda-Lime Glasses. A series of *in situ* XPS spectra under heating were shown in Figure 1(a)–1(f) where each XPS scanned the binding energy range of the photoelectron from 379 down to 363 eV at the sample temperature range from 20 to 450°C. The origin of the core level photoelectron of the element was labeled at each peak position. Not only do the binding energies of the silver peaks continuously shift, but also the line shapes of the peak change as the heating temperature increases.

In order to investigate the chemical states of silver during heating, a pure silver foil with native oxide on it was studied by ion sputtering and the XPS. The XPS spectrum of silver with silver oxide was shown in Figure 2(a) where the oxidized silver was found. Only metallic silver was seen in the XPS spectrum after 1 h of 2.8 keV argon ion sputtering shown in Figure 2(b). The binding energies and the FWHMs of oxidized silver, and metallic silver of $Ag3d_{5/2}$ and $3d_{3/2}$ peaks are listed in Table 1. The FWHMs of $Ag3d_{3/2}$ and $3d_{5/2}$ peaks

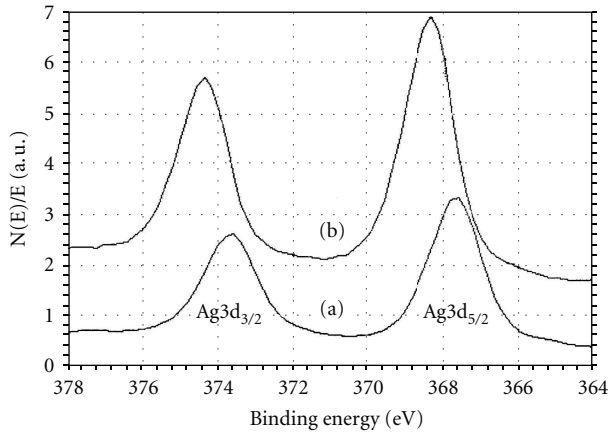

Figure 2: The XPS spectra of $Ag3d_{3/2}$ and $Ag3d_{5/2}$ from pure silver with native oxide (a) before sputtering and (b) after 1 h of argon ion sputtering.

Table 1: The variations of FWHM and binding energy shifts of metallic silver and oxidized silver of $Ag3d_{3/2}$ and $Ag3d_{5/2}$.

States	Peak	FWHM (eV)	Binding energy (eV)
Oxidized	$3d_{3/2}$	1.62	373.61
Oxidized	$3d_{5/2}$	1.68	367.61
Metallic	$3d_{3/2}$	1.51	374.32
Metallic	$3d_{5/2}$	1.55	368.32

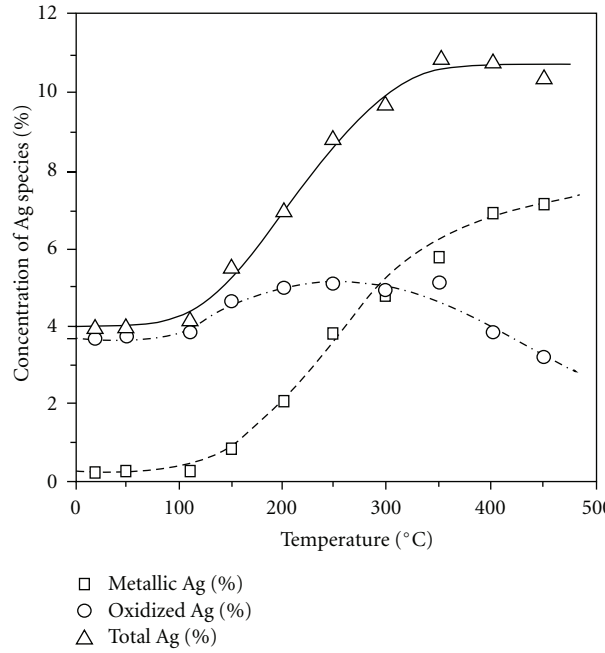

Figure 3: The concentration changes of total, metallic, and oxidized Ag on surface at different sample temperatures. A three-step diffusion process was observed.

of metallic silver are 1.51 eV and 1.55 eV, and those of $Ag3d_{3/2}$ and $3d_{5/2}$ peaks of oxidized silver are 1.62 and 1.68 eV. It is clear that the line width of metallic silver is smaller than that of oxidized silver, and the binding energy of metallic silver is approximately 0.6 eV higher than that of oxidized silver which is consistent with the results in the literature [13]. By comparing the data listed in Table 1 and Figure 1, it is clearly seen that the metallic silver on the surface gradually increases and becomes the dominant state during the heat treatment. In other words, more Ag–O bonds break and more metallic silver is formed on the surface during the heat treatment.

The metallic, Ag°, and oxidized silver, Ag^{+}, components in the Ag3d spectra shown in Figure 1, are decomposed by using a best Gaussian curve fitting program. The two chemical states of silver, Ag° and Ag^{+}, obtained from sputtering results in Table 1 were used as a guide to fit the spectra. The relative Ag concentrations including total, oxidized, and the metallic Ag during heating were calculated and plotted in Figure 3. A three-step growth of total Ag on the surface is clearly seen. Under 100°C the growth rate is low, then the Ag grows rapidly until 350°C, and finally it slows down. The oxidized Ag increases a little before 250°C and then decreases till 450°C, while the accumulation of metallic Ag shows a similar three-step pattern as the total Ag does.

It is clearly shown in Figure 1 that silver inside the ion-exchanged sample diffuses towards the surface during the heat treatment. Two chemical states of silver, Ag° and Ag^{+}, were resolved by comparing the line shapes of the Ag3d signals at various sample temperatures to the Ag3d spectra obtained from the sputtering of a pure silver metal. The growth of the higher binding energy component of the Ag3d signal indicates that the metallic silver is formed during heating.

The accumulation of silver on the surface was produced by Ag–O bond breaking during heating. This bond breaking in ion-exchanged sample results from the difference in Gibbs free energies of pure silver, silver oxide and SiO_2. Even though the Gibbs free energy of silver oxide (-2.68 kcal mol^{-1} at 25°C) is lower than that of pure silver (0 kcal mol^{-1} at 25°C) and higher than that of SiO_2 (~ -200 kal mol^{-1} at 25°C), the dissociation of oxygen from Ag–O bonds to form Si–O and Ag–Ag bonds still results in a net loss in the system energy [14]. Combining this energy loss and the thermal relaxation of the surface stress introduced by the size difference between Ag^{+} and Na^{+} (the ratio of ionic radii, $r_{Ag^{+}}/r_{Na^{+}}$, is 1.29) [15, 16] during the ion-exchange process, surface diffusion, and accumulation of metallic silver are clear. That is to say that the Ag–O bond breaking and the Ag–Ag and Si–O bond formation are thermodynamically favorable. Thus, the oxidized silver inside the glass network diffuses to the surface and then precipitates in order to maintain the system at a minimum energy state. Since a slight amount of metallic silver on the surface after the ion-exchange process and before heat treatment was observed, these metallic silvers can serve as nuclei for the precipitation.

The new Si–O bond formation on the surface was confirmed by the line shape changes and the positive binding energy shifts of O1s and Si2p XPS peaks which were described and discussed elsewhere [17]. These metallic silver

clusters in ion-exchanged glass were also found by Fourier transform IR spectroscopy [18].

The oxidized silver is involved in the diffusion process through the same diffusion mechanism as sodium inside alkali oxide glasses [19]. Only a few oxidized silvers have enough energy to move towards the incompletely relaxed surface at low temperature; hence, little metallic silvers are seen. Once the temperature is high enough (above 100°C), many Ag–O bonds are broken as the result of a more relaxed surface and consequently, more Ag° is precipitated. It is seen that the metallic silver is dominant product of the diffusion at sample temperature above 300°C. As more metallic silver and oxidized silver accumulate on the surface, either a repulsive potential must be generated which retards further diffusion or no more room for the silver to accommodate on the sample surface. This explains not only why the oxidized silver starts decreasing at 250°C but also the enrichment of total silver apparently slows down at temperature above 350°C.

3.2. Aluminum-Doped Zinc Oxide Films. Figure 4 shows the crystalline orientations of the as-deposited AZO film and films after annealed at 100, 200, 300, and 400°C observed *ex situ* by XRD. Even though a small (100) and big (002) peaks were observed between 26° and 40° as shown in Figure 4(a), only the obvious changes in (002) peak caused by the annealing were reported here. The changes of (002) peak measured by XRD *in situ* during annealing at specific temperatures were published previously [11]. It was seen that the diffraction angles changed as a function of annealing temperature in Figure 4. The double diffraction angle, 34.18°, was found in the as-deposited film; not much change in the double diffraction angles after 100, 200, and 300°C annealing which were 34.14°; 34.16°; and 34.16°, respectively. However, a big shift to 34.42° was observed in the film after 400°C annealing. The corresponding d-spacing, lattice constant, between two adjacent (002) crystalline planes was calculated by using the Bragg diffraction equation. The d-spacing in the film after being annealed at different temperatures was listed in Table 2.

The other feature in Figure 4(b) was that the intensity of the peak varied as a function of annealing temperature, very intense peak in as-deposited film, about the same but lower peak height seen in the films after annealed at 100, 200, and 300°C, and the lowest peak height after film annealed at 400°C. These peak heights as a function of annealing temperature were different when the XRD spectra were measured *in situ* at specific annealing temperatures reported previously [11] in which the peak intensity grew slowly when the annealing temperature was below 250°C but grew rapidly after 250°C. Since the intensity of the XRD peak indicates the quality of the crystallinity, a good quality of crystallinity in as-deposited film was seen, but the quality is getting worse after annealing. Energy provided by annealing activates the rearrangement of the atoms in the lattice which results in the changes of crystallinity. A significant amount of smaller Al^{3+} ions (74–104 pm radius [20]) substitute bigger Zn^{2+} ions (74–104 pm radius [20]) after 400°C annealing may result in the change in local strain, the reduction of the lattice constant, and the change of the crystalline quality.

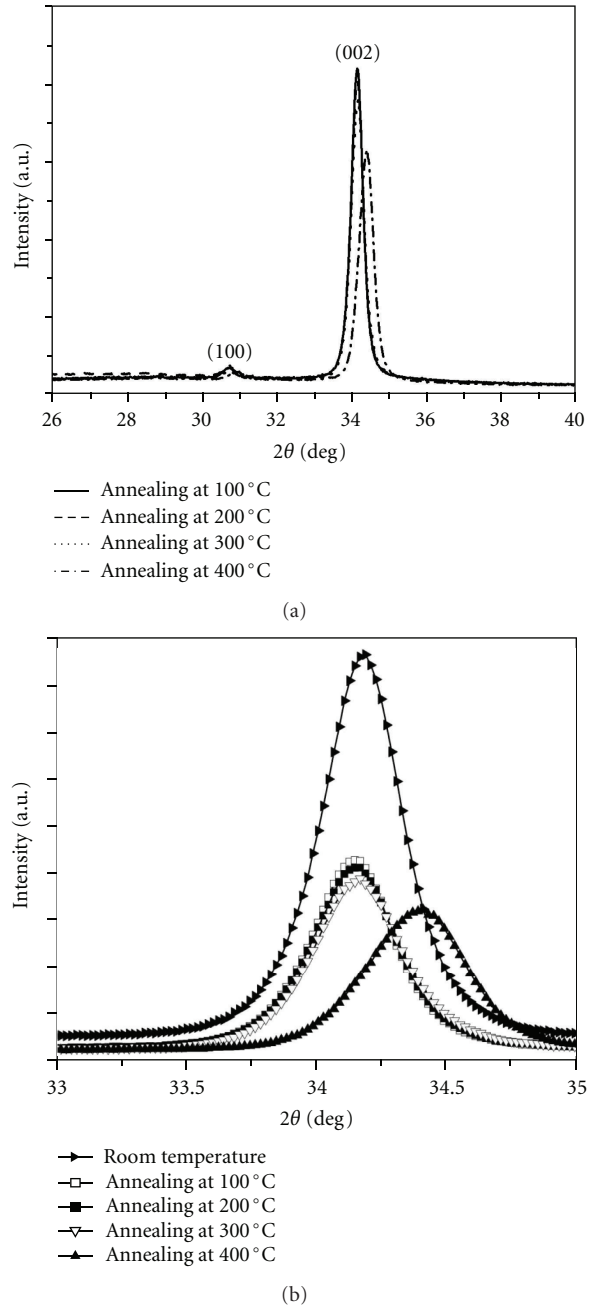

Figure 4: The XRD spectra of AZO films before and after annealing at various temperatures. (a) One small (100) and one big (002) peaks were observed in a range of 26° to 40° and (b) detailed variation of (002) peak as a function of annealing temperature.

From the analyses of the XRD peak shapes in Figure 4(b), the grain sizes along (002) orientation can be calculated by using the FWHM of the peak and the Scherer's formula. Both the FWHMs and the grain sizes were plotted in Figure 5 in which the higher the annealing temperature, the smaller the grain size was detected, that is, the smaller the grain size, the worse the quality of the crystallinity. The growth of the grain was expected after annealing but the opposite was observed. When the XRD spectra measured *in situ* at 400°C

Table 2: The d-spacing between (002) planes in AZO films under different conditions.

Film condition	2θ (°)	d-spacing (Å)
As-deposited at room temperature	34.18	2.621
After 100°C annealing and cooling down to room temperature	34.14	2.624
After 200°C annealing and cooling down to room temperature	34.16	2.623
After 300°C annealing and cooling down to room temperature	34.16	2.623
After 400°C annealing and cooling down to room temperature	34.42	2.603

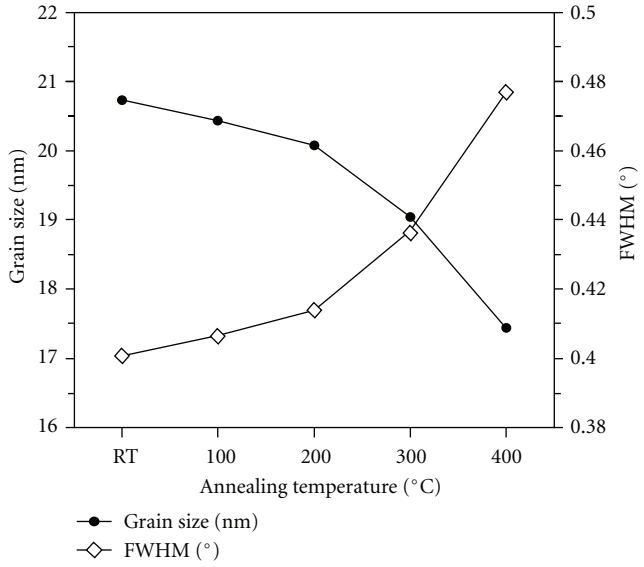

Figure 5: The grain sizes and FWHMs of the AZO films before and after annealing at different temperatures.

the replacement of Zn^{2+} by Al^{3+} occurred, and the increase of the grain size was observed in previous study [11]. However, when the spectra were collected *ex situ* after annealing at 400°C and cooling down to room temperature, the stress was greatly released as shown below. Cracks of the film were observed visually which resulted in the decrease of the grain size in the film. The thermally activated replacement of Zn^{2+} by Al^{3+} ions still remained in the film hence the reduction of the d-spacing was still detected.

The thermal energy may enhance or reduce the stress in the film which influences the rearrangement of the atoms in the film during the annealing. It is important to calculate the stress in the film after annealing. A biaxial strain model [21] was applied to calculate the stress in the films. The strain in the c-axis direction determined by XRD is $\varepsilon = (C_{film} - C_0)/C_0$, where C_0 is the unstrained lattice parameter from the ZnO powder, and C_{film} is the lattice constant of the film obtained from XRD spectra. The stress σ_{film} parallel to

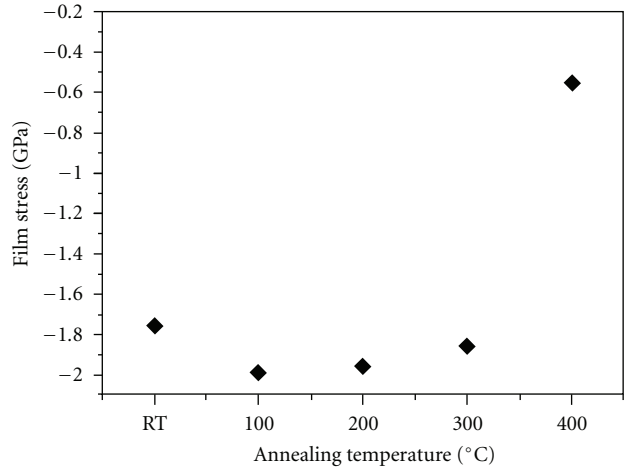

Figure 6: The compressive stress in the AZO film before and after annealing at different temperatures.

the film surface can be calculated by using the following formula, which is valid for the hexagonal lattice [22]:

$$\sigma_{film} = \frac{2c_{13}^2 - c_{33}(c_{11} + c_{12})}{2c_{13}} \times \frac{C_{film} - C_0}{C_0}. \quad (1)$$

For elastic constants c_{ij}, data of single ZnO crystalline have been used: $c_{11} = 208.8$, $c_{12} = 119.7$, $c_{13} = 104.2$, $c_{33} = 213.8$ GPa. The final equation of the film stress derived from XRD is deduced

$$\sigma_{film} = -233 \cdot \varepsilon(\text{GPa}). \quad (2)$$

The negative sign in above equation indicates that the stress in the film is compressive stress. The compressive stress determined from the above formula as a function of the annealing temperature is shown in Figure 6. It was found that the stress increases little after 100°C annealing and then decreases little after 200 and 300°C annealing, but there are a huge decrease in stress after 400°C annealing and cooling down to room temperature. From the calculation, there is about 1.8 Gpa compressive stress in the film after the deposition at room temperature by IBSD method. This compressive stress in the film was mainly caused by the kinetic energy loss of sputtered species, the film's structure, and the surface energy difference between the film and glass substrate.

Recent study of glass substrate temperature during sputtering deposition of aluminum by Sebag et al. [23] found that the substrate temperature rose in a range of 2 to 7°C during *ca.* 100 s time interval at the beginning of the deposition. Since the temperature risen was so low, there is no thermal effect on the deposited film fabricated by the IBSD method. The sputtered species with an energy ranged typically from a few eV to tens eV lost their energies from the momentum transfer process but no thermal annealing involved during the film growth on the substrate using IBSD method. A good quality of crystallinity in as-deposited film may attribute to this high compressive stress. The change

of compressive stress in the film after the annealing results from thermally activated replacement of bigger Zn^{2+} ions by smaller Al^{3+} ions and the formation and interaction of defects, vacancies, and interstitials. Once the compressive stress was greatly released after the 400°C annealing, the grain shrunk significantly due to the cracks of the film, that is, bigger grains were cut into small pieces. It was found that the resistivity and energy band-gaps of the AZO films are correlated well to the film structure [24].

4. Conclusion

Two case studies of Ag in ion-exchanged glasses and Al-doped ZnO films during and after heat treatment clearly demonstrate the thermal effect on the structural changes in both materials. The XPS and XRD were used to monitor the *in situ* and *ex situ* structural modifications of the Ag in ion-exchanged layer and AZO films. Two chemical states of Ag resulted from the reduction of the total Gibbs energy and the stress relaxation were found during annealing. By understanding how the metallic Ag formed and accumulated during annealing, an optimum heat treatment to grow the proper size and density of silver quantum dots in the films is possible. Postannealing effect on the AZO films shows that the crystallinity of the film decreases as the annealing temperature increases while the peak position shifts toward to higher diffraction angle, and grain size decreases dramatically after 400°C annealing due to cracks in the film. All the observed property changes can be explained by the thermally activated Zn^{2+} ions replacement by Al^{3+} ions and the compressive stress in the film.

Acknowledgment

Paul W. Wang acknowledges the support from a special emphasis research grant of Bradley University.

References

[1] J. L. Smith, G. M. Russel, and S. C. Bhatia, *Heat Treatment of Metals*, Alkem, Singapore, 2009.

[2] A. H. Al-Bayati, K. G. Orrman-Rossiter, J. A. van den Berg, and D. G. Armour, "Composition and structure of the native Si oxide by high depth resolution medium energy ion scatering," *Surface Science*, vol. 241, no. 1-2, pp. 91–102, 1991.

[3] A. J. Murrell, E. J. H. Collart, M. A. Foad, and D. Jennings, "Process Interactions between Low-energy Ion Implantation and Rapid-thermal Annealing for Optimized Ultrashallow Junction Formation," *Journal of Vacuum Science and Technology*, pp. 462–467, 2000.

[4] A. Ueda, R. Mu, Y. S. Tung et al., "Interaction of Fn-centers with gold nanocrystals produced by gold ion implantation in MgO single crystals," *Nuclear Instruments and Methods in Physics Research B*, vol. 141, no. 1–4, pp. 261–267, 1998.

[5] J. P. Zhao, Y. Meng, D. X. Huang, W. K. Chu, and J. W. Rabalais, "Sn quantum dots embedded in Si O2 formed by low energy ion implantation," *Journal of Vacuum Science and Technology B*, vol. 25, no. 3, pp. 796–800, 2007.

[6] A. Portavoce, R. Hull, M. C. Reuter, and F. M. Ross, "Nanometer-scale control of single quantum dot nucleation through focused ion-beam implantation," *Physical Review B*, vol. 76, no. 23, Article ID 235301, 2007.

[7] L. Chen, Z. Q. Chen, C. Liu, and Q. Fu, "Effect of annealing temperature on density of ZnO quantum dots," *Solid State Communications*, vol. 137, no. 10, pp. 561–565, 2006.

[8] K. Fukumi, A. Chayahara, N. Kitamura et al., "Chemical state and refractive index of Mg-ion-implanted silica glass," *Japanese Journal of Applied Physics*, vol. 41, no. 12, pp. 7447–7452, 2002.

[9] G. M. Renlund, S. Prochazka, and R. H. Doremus, "Silicon oxycarbide glasses: part II. Structure and properties," *Journal of Materials Research*, vol. 6, pp. 2723–2734, 1991.

[10] J.-C. Hsu, P. W. Wang, and C.-C. Lee, "X-ray photoelectron spectroscopy study of thin TiO2 films cosputtered with Al," *Applied Optics*, vol. 45, no. 18, pp. 4303–4309, 2006.

[11] Y.-Y. Chen, J.-C. Hsu, P. W. Wang, Y.-W. Pai, C.-Y. Wu, and Y.-H. Lin, "Dependence of resistivity on structure and composition of AZO films fabricated by ion beam co-sputtering deposition," *Applied Surface Science*, vol. 257, no. 8, pp. 3446–3450, 2011.

[12] C. T. Chang, J. C. Hsu, P. W. Wang, and Y. H. Lin, "ZnO thin films deposited with various oxygen partial pressures by ion beam sputtering at room temperature," in *Proceedings of the International Conference on Optics and Photonics in Taiwan (OPT '08)*, National Chiao Tung Unversity, Taiwan Optical Engineering Society, Taipei, Taiwan, 2008, Fri-P1-044.

[13] J. S. Hammond, S. W. Gaarenstroom, and N. Winograd, "X-ray photoelectron spectroscopic studies of cadmium- and silver-oxygen surfaces," *Analytical Chemistry*, vol. 47, no. 13, pp. 2193–2199, 1975.

[14] D. R. Lide, *CRC Handbook of Chemistry and Physics*, CRC press, Boca Raton, Fla, USA, 1991.

[15] S. S. Kistler, "Stresses in glass produced by nonuniform exchange of monovalent ions," *Journal of the American Ceramic Society*, vol. 45, no. 2, pp. 59–68, 1962.

[16] R. C. West and M. J. Astle, *CRC Handbook of Chemistry and Physics*, CRC Press, Boca Raton, Fla, USA, 1981.

[17] P. W. Wang, "Thermal Stability of Silver in Ion Exchanged Soda Lime Glasses," *Journal of Vacuum Science and Technology*, vol. A14, pp. 465–470, 1996.

[18] N. A. Sharaf, R. A. Condrate, and A. A. Ahmed, "FTIR spectral/structural investigation of the ion exchange/thermal treatment of silver ions into a silicate glass," *Materials Letters*, vol. 11, no. 3-4, pp. 115–118, 1991.

[19] J. R. Johnson, R. H. Bristow, and H. H. Blau, "Diffusion of Ions in Some Simple Glasses," *Journal of the American Ceramic Society*, vol. 34, pp. 165–172, 1951.

[20] J. E. Huheey, *Inorganic Chemistry: Principles of Structure and Reactivity*, Harper Collins, New York, NY, USA, 1983.

[21] A. Segmuller, M. Murakami, and R. Roscoberg, *Analytical Techniques for Thin Films*, Academic Press, Boston, Mass, USA, 1988.

[22] R. Cebulla, R. Wendt, and K. Ellmer, "Al-doped zinc oxide films deposited by simultaneous rf and dc excitation of a magnetron plasma: relationships between plasma parameters and structural and electrical film properties," *Journal of Applied Physics*, vol. 83, no. 2, pp. 1087–1095, 1998.

[23] J. Sebag, J. Andrew, D. Neill, and M. Warner, "Substrate temperature and strain during sputter deposition of aluminum on cast borosilicate glass in a Gemini Observatory coating chamber," *Applied Optics*, vol. 49, no. 24, pp. 4610–4620, 2010.

[24] Y.-Y. Chen, J.-C. Hsu, C.-Y. Lee, and P. W. Wang, "Post-annealing Properties of Aluminum Doped Zinc Oxide Films Fabricated by Ion Beam Co-sputtering," in *Proceedings of the 11th International Symposium on Sputtering and Plasma*, Kyoto, Japan, July 2011.